Journal of
Composites Science

MDPI

Article

Experimental Investigation to Optimize the Manufacturing Parameters of Ankle–Foot Orthoses Using Composite and Titanium Nanoparticles

Najlaa J. Khalaf [1,2], Sabrine Ben Amor [2], Borhen Louhichi [2,3,*], Jumaa S. Chiad [1] and Abdennour Seibi [4]

1 Mechanical Engineering Department, College of Engineering, Al-Nahrain University, Baghdad 10072, Iraq; najla.jasim1@gmail.com (N.J.K.); jumaa.s.chiad@nahrainuniv.edu.iq (J.S.C.)
2 Mechanical Laboratory of Sousse, Higher Institute of Applied Science and Technology of Sousse, University of Sousse, Sousse 4000, Tunisia; sabrinebenamor94@gmail.com
3 Department of Mechanical Engineering, College of Engineering, Imam Mohammad Ibn Saud Islamic University (IMSIU), Riyadh 11432, Saudi Arabia
4 Department of Engineering, Utah Valley University, 800 W University Pkwy, Orem, UT 84058, USA; aseibi@uvu.edu
* Correspondence: blouhichi@imamu.edu.sa; Tel.: +966-55-355-6733

Abstract: The optimum structural characteristics of lamination materials used in the fabrication of prosthetic and orthotic parts were investigated in this work. Optimization was chosen based on high yields, ultimate stresses, and bending stress properties. The ideal materials were determined through the use of an RSM (response surface methodology) which considers three factors: Perlon reinforcement, a layer of glass fiber, and the percentage of titanium nanoparticles combined with the matrix laminating resin. The RSM approach suggests thirteen samples by manipulating two variables: the Ti nano percentage and the number of Perlon layers. Laminating materials, defined by RSM methods and treated with a vacuum system, were submitted to a series of tests. The ideal lamination material was compared with the laminations from the initial study through the use of tensile, flexural, and fatigue testing according to ASTM standards. Tests carried out using version 10.0.2 of Design Expert software showed that, compared with the 12 other laminations, the one with 10 Perlon layers and 0.75 percent Ti nano had the highest overall yield and ultimate and bending loads. Fatigue eventually showed that stamina tension constraints were applied for optimal lamination, compared to ten Perlon lamination layers. We additionally tested the fatigue life of the best material and compared it with the available materials used at prosthetics and orthotics centers.

Keywords: ankle–foot orthoses; mechanical properties; RSM method; composite; Perlon layers; titanium nanoparticle

Citation: Khalaf, N.J.; Ben Amor, S.; Louhichi, B.; Chiad, J.S.; Seibi, A. Experimental Investigation to Optimize the Manufacturing Parameters of Ankle–Foot Orthoses Using Composite and Titanium Nanoparticles. *J. Compos. Sci.* **2024**, *8*, 45. https://doi.org/10.3390/jcs8020045

Academic Editors: Jeevithan Elango, Kandasamy Saravanakumar and Wenhui Wu

Received: 28 November 2023
Revised: 19 December 2023
Accepted: 27 December 2023
Published: 25 January 2024

1. Introduction

Researchers have recently shown increasing interest in prosthetics and orthotics due to the large number of patients who have lost a limb through an amputation or a congenital malformation. A prosthesis is a synthetic substitute for a body part that is missing, whereas an orthosis is an artificial tool designed to increase the potential of a body part, such as reducing pain, repairing deformities, improving organs, aiding mobility or augmenting weak muscles, regulating spastic muscles, and other functions [1].

Weight, durability, and personal recognition are all important, but cost and usability also matter greatly in determining the quality of an orthosis [2]. To meet these criteria, new technologies such as 3D printing can be used to manufacture orthoses [3,4]. The objective of orthosis is to improve the mobility of users and enable them to participate in functional tasks that are carried out regularly. The weight, lifespan, and material used are the principal factors that are considered for orthosis fabrication. There are two different categories of orthoses: static orthosis and dynamic orthosis. When fractures are treated with a static orthosis, mobility is restricted, and the device is a rigid support.

On the other hand, a dynamic orthosis is a device that increases body mobility and enables the optimal capacity of the organ, including the ability to recover and control joint movement [5]. The foot orthotic that is recommended by medical and physical specialists can help in the prevention of future troubles by lowering abnormal or pathological stresses that are operating on the lower extremity and the foot [6,7].

The ankle–foot orthosis, commonly known as AFO, is a rigid support device that is placed on the lower leg to ensure stability for both the ankle and the foot. This device allows users to keep their ankles in their normal position when walking or participating in other activities. Those who suffer from foot drop, often known as an inability to raise the foot, may frequently utilize an AFO to assist them in clearing their toes when walking [8]. AFOs are widely used in the treatment of illnesses that affect the functionality of the muscles, such as multiple sclerosis, cerebral palsy, muscular dystrophy, polio, and stroke [9]. Ankle–foot orthoses or prostheses are subject to fatigue and external loads. Therefore, it is important to study and improve the mechanical characteristics of the materials used in their manufacturing.

To improve the properties of orthoses and prostheses, innovative approaches involve exploring new materials and designs. The incorporation of nanomaterials, in particular titanium (Ti) nanoparticles, renowned for their exceptional mechanical properties, is a promising avenue for improvement. These nanoparticles have attracted a great deal of attention from scientific researchers, communities, and industries.

Ti nanoparticles have remarkable properties, including a favorable Young's modulus, exceptional flexibility, and high electrical and thermal conductivity [10]. The extraordinary mechanical properties of Ti nanoparticles also contribute to their appeal [11]. The integration of these nanomaterials into the manufacture of orthoses and prostheses aims to improve their overall performance, durability, and functionality. This is a progressive advance in the field, with potential implications for medical and industrial applications. This study focuses on the manufacturing and building of ankle–foot orthoses using composite structures reinforced by titanium nanoparticles. An experimental investigation is conducted for the optimization of two quantitative parameters: the number of layers of the Perlon fiber and the percent of titanium nanoparticles combined with the matrix resin. These parameters enable us to obtain the best structure of the AFO supporting the maximum stress.

In this context, the stress analysis and the mechanical properties of knee sockets were studied by Al-Shammari et al. [8] using both numerical and experimental techniques. Abbas et al. [12] studied a partial foot made of various composite materials to determine its fatigue behavior. The photo-elasticity approach was utilized by Yaseen [13] to determine the distribution of stress in the knee joint, which was then compared with the numerical data. Takhakh et al. [14] investigated the mechanical characteristics of reinforced carbon fibers in a foot orthosis. Yousif et al. [15] employed both experimental methods to estimate the mechanical characteristics of the newly designed foot and computational methods to investigate the mechanical behavior of the foot depending on temperature. Computational modeling of the mechanical performance of the foot was followed by an experimental investigation of the composite materials' mechanical properties by Oleiwi et al. [16]. Then, Kadhim et al. [17] employed a combination of both numerical and experimental methods to investigate how including nanoparticles influences both the overall performance and mechanical characteristics. The impact of carbon nanoparticles on the dynamic performance of composite materials was investigated by Abbas et al. [18] using both numerical and analytical methods. In the same context, the impact of carbon nanoparticles on rubber creep performance was then studied using experimental methods by Abdulridha et al. [19]. In addition, experimental research into the impact of nanoassembly on the mechanical characteristics of composite materials was also carried out by Taher et al. [20]. Oleiwi et al. [21] studied numerous mechanical characteristics, such as weariness, roughness, and the effect of heat, to investigate the impact of nanoparticle-based materials on the architecture of the hip joint. In addition, Salih et al. [22] used an experimental technique to study rubber materials' mechanical properties under the effect of nanomaterials and fiber reinforcement. Using a maxillofacial application, in a second study carried out by the authors [23], the effect of nanoparticles on the mechanical characteristics of silicone rubber was investigated. The effects of nanoparticles on mechanical characteristics and bioimplants were studied by Mohammed et al. [24]. Al-Waily [25] used analytical and numerical methods to study the effect of nanoparticles on the thermal distortion properties of composite materials.

Ankle–foot orthoses (AFOs) fulfill several functions and must therefore be as easy and comfortable as possible to use. The material must not only be low-cost but also have high-quality mechanical properties. Due to the complex shape of the leg and ankle, the researchers utilized 3D modeling and printing to design and manufacture the device. Rogati et al., 2022 [26] evaluated the repeatability of newly constructed equipment used to test the stiffness of ankle–foot orthoses (AFOs) under ideal frictionless circumstances. Shahar et al., 2022 [27] studied the thermal and physical properties of natural composite filament made from kenaf and polylactic acid (PLA) and investigated its potential as a material for making ankle–foot orthoses (AFOs) through the use of 3D printing.

In the same context, Patel et Gohil [28] presents a comprehensive review of the AFO design and development process, using advanced manufacturing techniques. The AFO component was manufactured using PLA material on an FDM printer. Yje production time for a single 3D-printed personal device is less than 6.5 h. Gupta et al. [29] reviewed the design process for a 3D-printed ankle–foot orthosis for podiatric applications, focusing on time and cost-effectiveness. The work also discusses biomechanical control parameters and advances in 3D printing, demonstrating the biocompatibility of wearable and implanted products. Caravaggi et al. [30] present a full report on the design and production process of a unique PD-AFO (posterior leaf spring ankle–foot orthosis) made from glass-fiber-reinforced polyamide. The viability of the proposed method was examined for a 67-year-old patient with foot drop following paraparesis caused by severe discarthrosis after spinal stabilization surgery. In another study, Khandagale et Pise [31] aimed to manufacture an ankle–foot orthosis (AFO) using composite materials to increase its strength and durability. Due to the complex nature of the ankle and leg section, they opted for 3D modeling and printing to facilitate the design and production process for this specific component. Willis et al. [32] present the process of creating and constructing an external orthotic device, specifically designed to correct mild to moderate cases of hallux valgus (HV), often known as bunions, without the need for invasive procedures. Two orthopedic models made from composite materials were developed externally. Each model comprises a polymeric shell around the foot and two toes, together with a metal or carbon fiber insert that maintains the alignment of the big toe and generates resistance. The initial prototype was fabricated by utilizing 3D printing methodologies to verify the results.

This study aims to conduct an experimental investigation for the optimization of ankle–foot orthoses using composites along with nanoparticles of titanium. The paper is structured as follows. After this introduction, the different materials and methods used in this paper are presented. In Section 3, the experimental approach is described. The results and discussion are summarized in Section 4, while the conclusions and perspectives are presented in Section 5.

2. Materials and Methods

2.1. Materials

To conduct our experimental investigation and mechanical tests, we used the following materials to manufacture composite ankle–foot orthoses with titanium nanoparticles:

1. Stockinet made of Perlon (Ottobock Health Care 623T3) 1. The procedures of drawing and melting were used to create Nylon 6, also known as Perlon, Figure 1a.
2. Glass fiber (ottobock health care 616G13) as shown in Figure 1b.

3. Ti nanoparticles/nanopowders have an outer diameter (of 30–50) nm [33]; black grey and Ti nanoparticles should be avoided under stress, Figure 1c.
4. Lamination resin 80:20 polyurethanes (ottobock healthcare 617H19). Most commonly, a diisocyanate and a polyol react to produce polyurethane resin. The foams, elastomers, and fluids for coatings can be either flexible or rigid, depending on the application, Figure 1d.
5. Polyvinyl alcohol PVA bag (Ottobock Health Care 99B71). PVA to isolate the composite material around the mold and to put the matrix mixture between two PVAs, Figure 1e.
6. Powder is used to harden the composite material (ottobock health care 617P37), Figure 1f.

Figure 1. Materials for manufacturing AFO laminations: (**a**) white Perlon stockinet, (**b**) glass fiber (**c**) Ti nanoparticles, (**d**) polyurethane resin, (**e**) polyvinylalcohol PVA bag, and (**f**) hardening powder.

The main equipment used in the fabrication of the ankle–foot orthoses is shown in Figure 2 and described below:

1. One gypsum mold is a parallelogram with the following dimensions: ($20 \times 12 \times 24$ cm^3), Figure 2a.
2. Vacuum device containing a vacuum pump, pipes, and a suction hood. The two major uses for this device are to make a mold free of bubbles by creating a space between the PVA and the mold and to create a cast free of bubbles by creating a space between two PVA bags.
3. The university's Center for Nanotechnology Research made use of three different kinds of ultrasonic equipment: an ultrasonic mixing device, an ultrasonic device of the Hielscher type, and an ultrasonic processor (UP200Ht). Ti nanoparticles and polyurethane resin with varying weight percentages (0, 0.25, 0.5, 0.75, and 1) may be mixed using ultrasonic equipment consisting of an ultrasonic generator, a probe, and

settings of 26 kHz and 160 Watt for 60 min [11]. The mixing procedure was carried out following the suggestions for risk minimization provided by the Cheap Tubes Company [34].

4. A sensitive scale device with three digits that are used to weigh Ti nanoparticles and calculate the physical properties of the composite material, Figure 2f.

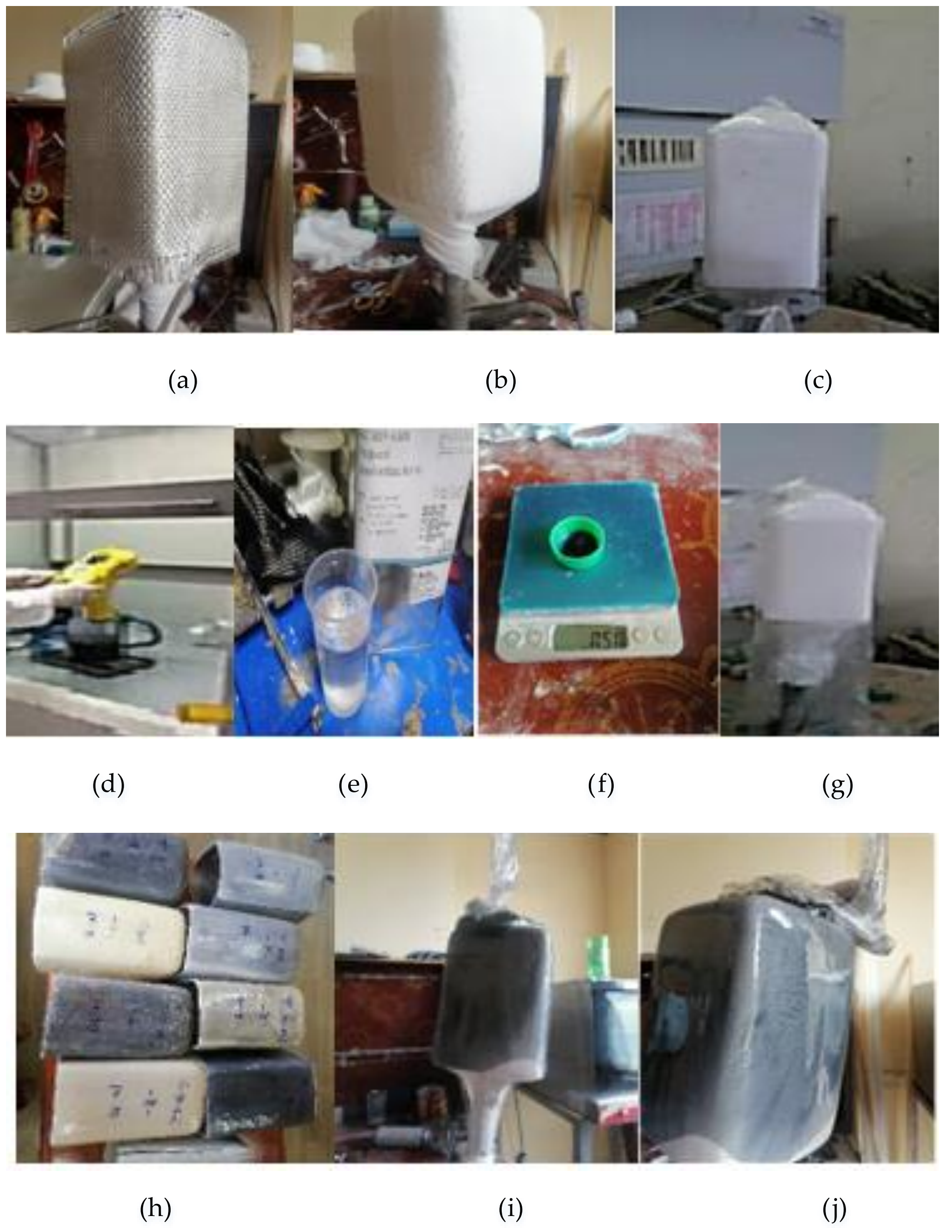

Figure 2. Specimens' preparation by the vacuum method: (**a**) first PVA with the gypsum mold, (**b**) Perlon layers, (**c**) fiberglass, (**d**) second PVA above the Perlon layers, (**e**) nano titanium weight %, (**f**,**g**) ti nano with the resin mixing process, (**h**,**i**) placing the matrix, and (**j**) the mold.

2.2. Response Surface Methodology (RSM)

The RSM methodology represents a synergistic mix between statistical and mathematical methods to build experimental models and to analyze problems where a desired response is affected by several parameters. The principal objective is to enhance this response through systematic experimentation. The RSM method is particularly effective for refining previous research and available products. Using precise experimental designs, the main objective is to identify an optimal solution (output variable) affected by several independent parameters (input variables). This methodology facilitates the exploration of the relationships between these variables, enabling researchers to identify the optimal conditions that lead to the desired results and improvements in the system or process under investigation. RSM methodology was employed for this analysis, with a composite central design over two factors, using five central points and $\alpha = \pm 2$. The experimental design matrix involves conducting thirteen runs, which include five central points. The parameter was tested with four different code levels: −2, −1, 0, 1, and 2. Each code level represents an actual value corresponding to the coded value. Ti nanoparticles and the number of Perlon layers are thus the input parameters investigated. Table 1 shows the input parameter levels and their corresponding codes. This model was created using the software DESIGN-EXPERT 10.0.2.

Table 1. Input parameter levels and their corresponding codes.

Factor	Unit	Low Level (−1)	High Level (+1)	−Alpha	+Alpha
Ti Nanoparticles	%	0.25	0.75	0	1
The number of Perlon layers	No. of layer	6	10	4	12

3. Experimental Approach

3.1. Ankle–Foot Orthoses Laminations with Design Parameters

The characteristic parameters of ankle–foot orthosis (AFO) laminations are determined through a consideration of practical insights and the limitations inherent in analytical methods. The selection of input parameters for the experiment is guided by practical knowledge and the constraints of analytical methodologies [35–41]. Therefore, the measured parameters are the number of Ti nanolayers and Perlon layers. The nano titanium percentages are in 80:20 lamination resin range from 0% to 1%, while for Perlon, the range is 4–12% across 13 trials (Table 2). The software Design-Expert 10.0.2 was employed to develop the blueprint. The specimens were cleaned and AFO orthicons were made through the use of a vacuum lamination process.

Table 2. Suggested experiments (runs) by the RSM.

Runs No.	Exp. No	Glass Fiber	Ti Nanoparticles in Code	Perlon (Layers) in Code	Ti Nanoparticles (%)	Perlon (Layers)
1	3	1	−1	−1	0.25	6
2	4	1	+1	−1	0.75	6
3	8	1	−1	+1	0.25	10
4	7	1	+1	+1	0.75	10
5	6	1	−2	0	0	8
6	5	1	+2	0	1	8
7	1	1	0	−2	0.5	4
8	9	1	0	+2	0.5	12
9	2	1	0	0	0.5	8
10	10	1	0	0	0.5	8
11	11	1	0	0	0.5	8
12	12	1	0	0	0.5	8
13	13	1	0	0	0.5	8

3.2. Mechanical Tests

The mechanical property tests, including the tensile test, bending test, and fatigue test, were carried out for all laminations.

3.2.1. The Tensile Test

The tensile test was carried out with the Testometric instrument shown in Figure 3. The dimensions and shape of each specimen were determined through the use of ASTM standard D638 [42]. Laser computer numerical control (CNC) was used to cut two different specimen types (I and IV) following the ASTM standard. Each specimen was subjected to testing with a strain rate of 2 mm/min, as illustrated in Figure 4.

Figure 3. Tensile test device (Testometric).

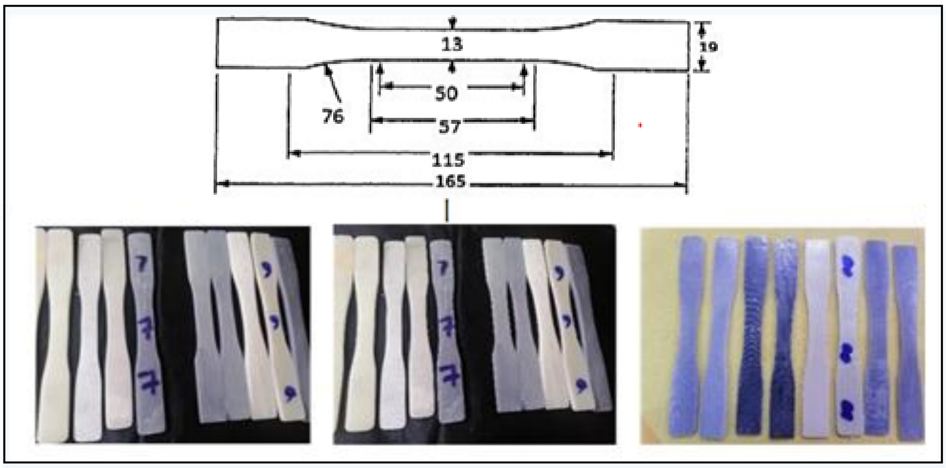

Figure 4. Tensile test specimens (type I).

3.2.2. Bending Test

The standardized measuring instrument (Testomertic) was used to measure the flexural strength of three samples from each lamination (run) as shown in Figure 5. Three crosshead speed samples at 5 mm/min with capacities of 25 kN were tested and analyzed (Figure 6) to find the optimal material for each lamination. The procedure followed ASTM D790-03 [43]. The equations presented below were used to calculate the flexural bending stress, the flexural strain, and the bending modulus [44]:

$$\sigma_f = \left(\frac{3PL}{2bd^2}\right)\left(1 + 6(\frac{D}{L})^2 - 4\left(\frac{d}{L}\right)\left(\frac{D}{L}\right)\right) \tag{1}$$

$$\varepsilon_f = \left(\frac{6Dd}{L^2}\right) \tag{2}$$

$$E_f = \left(\frac{\sigma_{f2} - \sigma_{f1}}{\varepsilon_{f2} - \varepsilon_{f1}}\right) \tag{3}$$

where:
σf: flexural bending stress (MPa)
εf: flexural strain
Ef: bending modulus (GPa)
P: force (N)
L: length (mm)
b: width (mm)
d: depth (mm)
D: deflection of the specimen's center line in the middle of the support span (mm)

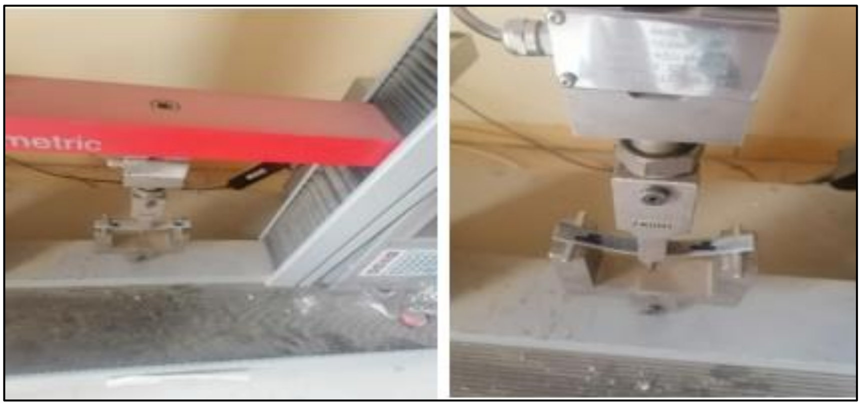

Figure 5. Bending test device universal instrument (Testometric).

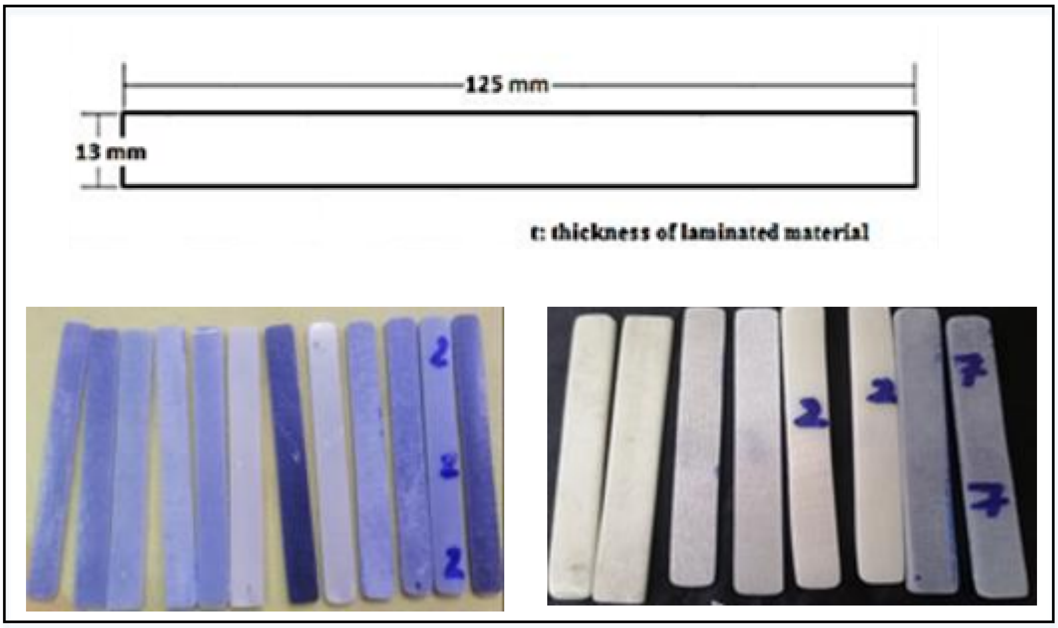

Figure 6. Bending test specimens.

3.2.3. The Fatigue Test

Fatigue represents the cumulative injury's periodic loading cycle. Only areas that plastically flex under the cyclical load are subject to fatigue damage. An HSM20 (High Speed Measuring Machine) as shown in Figure 7 was used to conduct the fatigue test. This device utilized the alternating bending motion with a rate of 24 rotations per second. The shape and dimensions of the specimens, as indicated in Figure 8, were produced following the machine manual [39]. Furthermore, all computations were carried out using their proper names as listed in the user guide. The optimal lamination content was determined by testing three specimens across seven stress levels. Then, the S-N curve and fatigue characteristics were compared with suitable laminating materials.

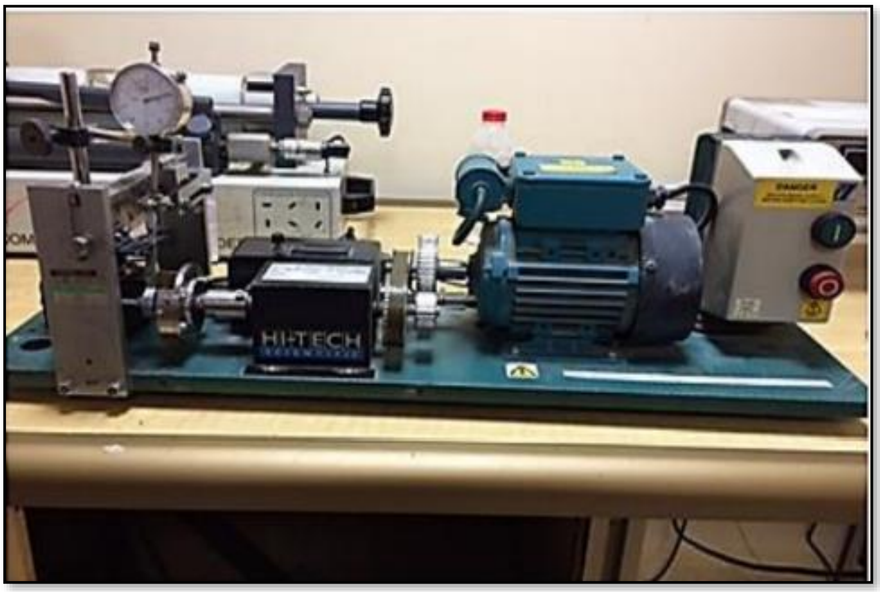

Figure 7. Alternating–bending fatigue testing machine (HSM20).

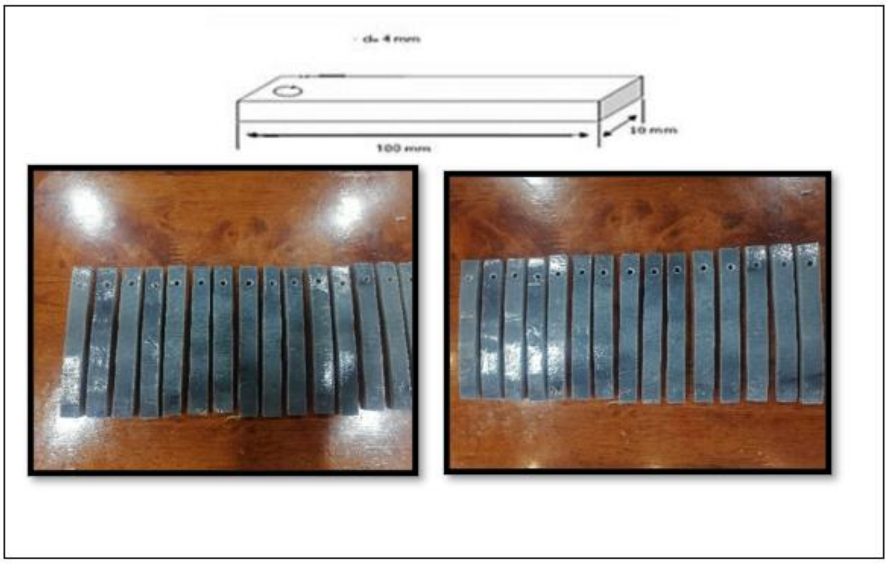

Figure 8. The fatigue test specimens.

4. Results and Discussion

4.1. The Physical Properties

For each lamination (runs), thickness, weight per unit area, density, and volume fraction were calculated as shown in Table 3. These results indicate that the mean weight and thickness are influenced by the number of Perlon layers, but the presence of Ti nanoparticles has no observable effect on the physical properties. Notably, the relation linking the number of layers of Perlon to the weight appears to be linear, highlighting a clear correlation. Interestingly, Ti nanoparticles do not significantly affect the overall weight, suggesting that their contribution can be considered negligible in comparison with the entire weight. Furthermore, the volume fraction value is contingent upon both thickness and weight, with its determination primarily tied to the number of Perlon layers. This underscores that Ti nanoparticles play a minimal role in influencing the volume fraction. In Figure 9, an image of the optimal material obtained by a scanning electron microscope (SEM) (comprising 0.75% weight of Ti nanoparticles and 10 Perlon layers) is presented, featuring two magnification levels (500× and 2000×). Figure 9 illustrates a high degree of cohesion between Ti nano and matrix material (polyurethane resin) and good dispersion of the Ti nano in the matrix material.

Table 3. Physical properties for all laminations (runs).

Runs No.	Exp. No	Fiber Glass	Titanium Nanoparticles (%)	Perlon (No. of Layer)	Thick (mm)	Density (g/cm^3)	Mass (g)	Volume (cm^3)	Weight per Unit Area (g/cm^2)
1	3	1	0.25	6	3	1.49333	7.28	4.875	0.448
2	4	1	0.75	6	2	1.64920	5.36	3.25	0.329
3	8	1	0.25	10	4	1.610769	10.47	6.5	0.644
4	7	1	0.75	10	5	1.441231	11.71	8.125	0.72
5	6	1	0	8	4	1.443077	9.38	6.5	0.577
6	5	1	1	8	4	1.338462	8.70	6.5	0.535
7	1	1	0.5	4	3	1.167179	5.69	4.875	0.35
8	9	1	0.5	12	4	1.446154	9.40	6.5	0.578
9	2	1	0.5	8	4.5	1.434529	10.49	7.3125	0.645
10	10	1	0.5	8	4.5	1.434529	10.49	7.3125	0.645
11	11	1	0.5	8	4.5	1.434529	10.49	7.3125	0.645
12	12	1	0.5	8	4.5	1.434529	10.49	7.3125	0.645
13	13	1	0.5	8	4.5	1.434529	10.49	7.3125	0.645

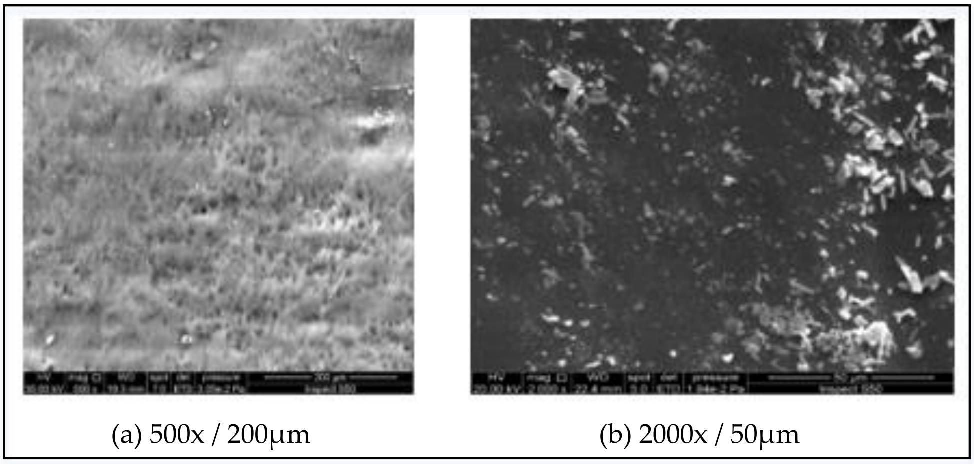

Figure 9. The optimal composite structure determined through the use of scanning electron microscopy (SEM) (0.75% weight of nano Ti and 10 Perlon layers) at two resolutions: (**a**) 200 µm and (**b**) 50 µm.

4.2. Results of Tensile Tests

At room temperature, a tensile test apparatus called a Testometric was used to evaluate three samples per run, and an average was then determined. Figure 10 reviews the counter graph of the nano Ti, the yield stress, and the Perlon layers as a response. Using two input parameters (weight percentage of Ti nanoparticles and no. of Perlon layers), the mechanical stresses and modulus of elasticity were determined. It was also shown that when the percentage of Ti nanoparticles was mixed with the matrix (lamination resin), the yield stress and other parameters improved. Ti nano's excellent stiffness and strength, high flexibility, coupled with its high flexibility and diameter-dependent specific surface area, and high aspect ratio combine to alter the properties of the lamination resin that contains it. Additionally, increasing the reinforcement material (Perlon fiber) in the composite materials increased the mechanical properties.

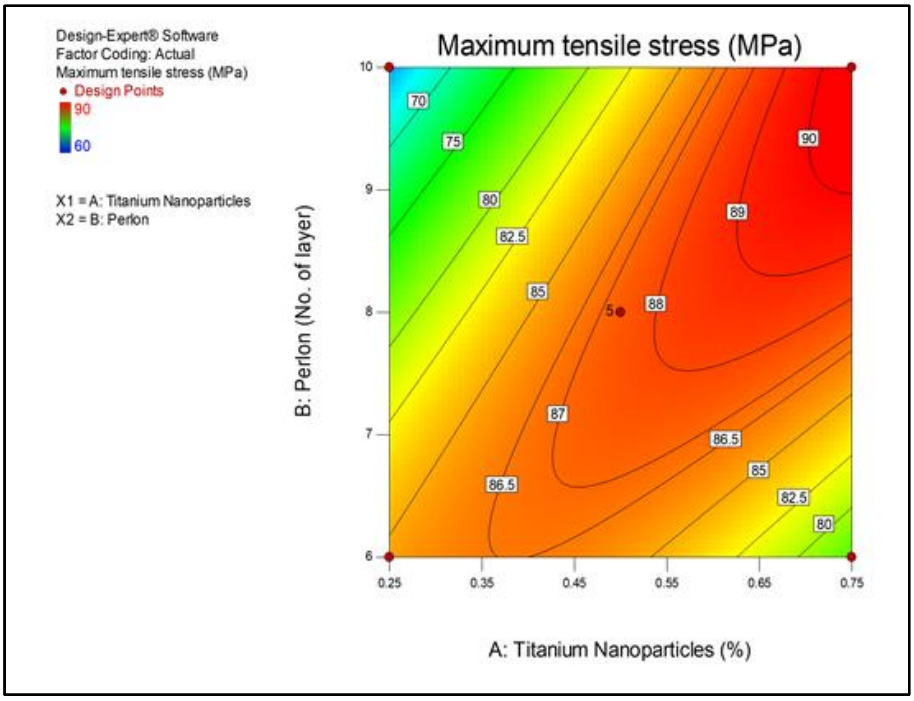

Figure 10. Contour graph of maximum tensile stress in terms of titanium nanoparticles and the no. of Perlon layers.

The final equation of maximum tensile stress in terms of actual factors is:

$$\begin{aligned}\text{Maximum tensile stress} = +78.01437 - 49.41379 \times \text{Titanium Nanoparticles} + 5.22989 \times \text{Perlon} + \\ 17.00000 \times \text{Titanium Nanoparticles} \times \text{Perlon} - 68.58621 \times \text{Titanium Nanoparticles}^2 - 0.91541 \times \text{Perlon}^2\end{aligned} \tag{4}$$

To predict maximum tensile stress, a quadratic model reduced to coded terms was examined by means of the reverse elimination of non-significant coefficients. The model demonstrates significance at a 95% confidence level. Notably, titanium nanoparticles (A), the number of Perlon layers (B), the interaction term (AB), and their respective squares have p-values below 0.05, representing their significance in the model. A decent model will fail the goodness-of-fit test. This model shows that the maximum tensile stress is most affected by the first three components and is only moderately affected by the fourth term (B).

Figure 11 presents the 3D plot (surface plot) of maximum tensile stress as a function of titanium nanoparticles and the no. of Perlon layers and validates the previous observations. It can be noted that the increase in both titanium nanoparticles and the no. of Perlon layers at their higher level resulted in an increase in the maximum tensile stress value due to their combined effect. In other words, this is properly ascribed to the same reason mentioned above. However, the titanium nanoparticle percentage has a higher impact than the no. of Perlon layers on the maximum tensile stress, while the lower levels (0.25% titanium nanoparticles and six as the no. of Perlon layers) reduced the value of maximum tensile stress. The residuals lying in a straight line, indicating errors, show a normal distribution, as shown in the plot of normal probability (Figure 12) for the maximum tensile stress data. Furthermore, no clear patterns or strange structures can be observed in the residuals compared to the projected responses for the data relating to maximum tensile stress (Figure 13), demonstrating that the models are valid.

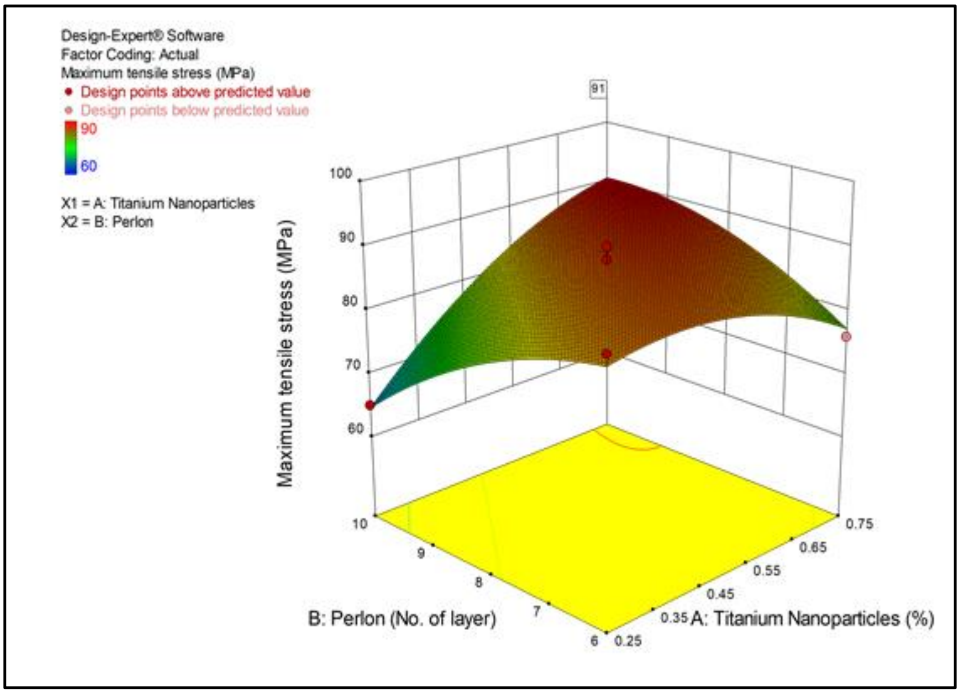

Figure 11. The 3D surface plot of tensile stress at the peak in terms of the titanium nanoparticles and the no. of Perlon layers.

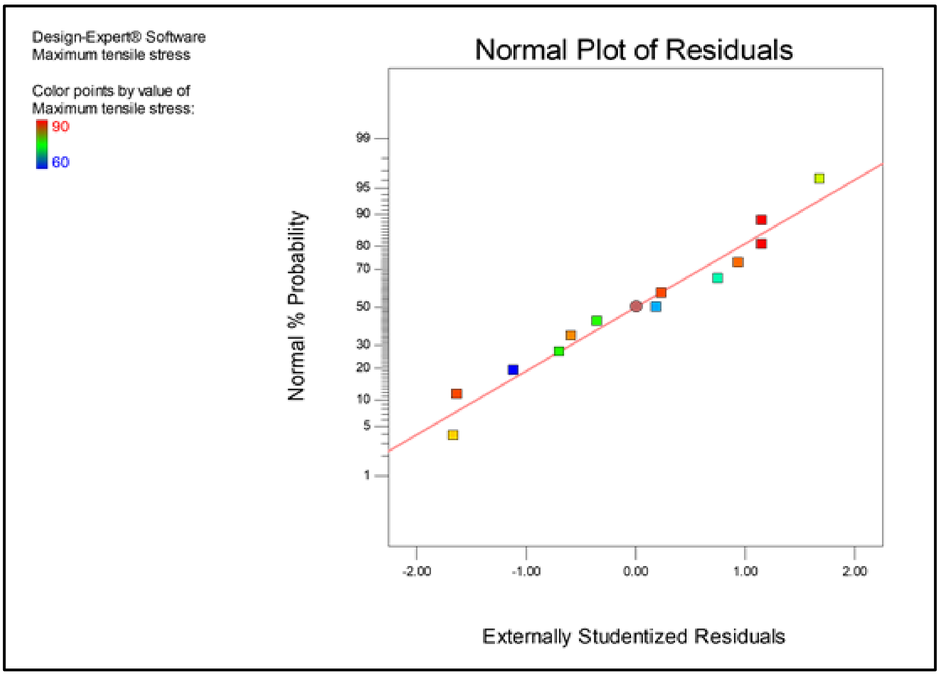

Figure 12. Plot of normal probability for the maximum tensile stress data.

For comparison, Figure 14 shows the predicted versus actual maximum tensile stress data, and Figure 15 shows the maximum tensile stress perturbation showing the effect of titanium nanoparticles and the number of Perlon layers on peak tensile stress across the range of levels used. Titanium nanoparticles have a greater impact on the maximum tensile stress than the number of Perlon layers, whereas Figure 16 indicates that the combined influence of the two input factors begins after the center (at around 0.55% titanium nanoparticles for a maximum tensile stress of around 85 MPa).

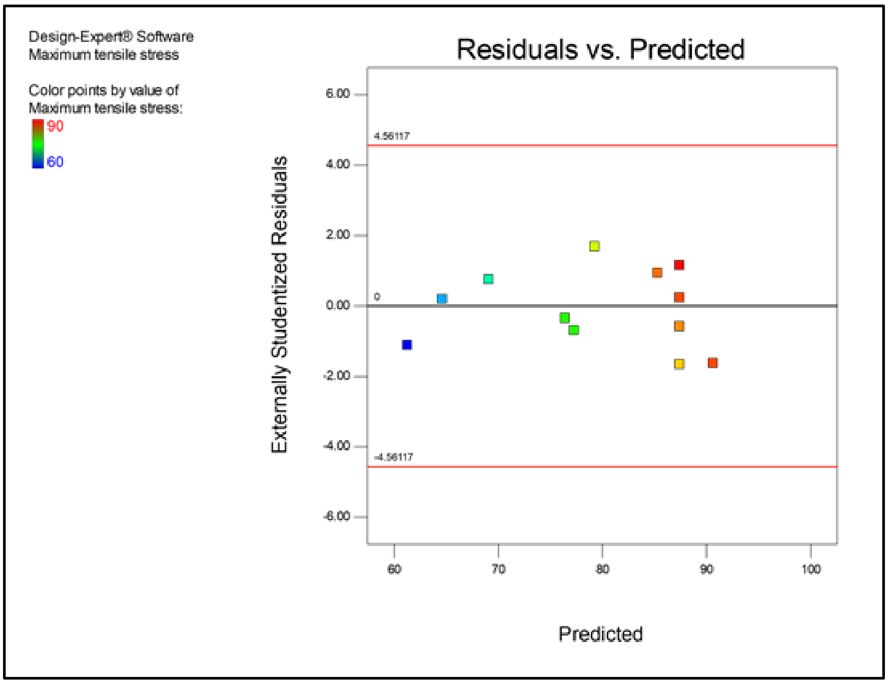

Figure 13. Plot of residuals of the maximum tensile stress versus the predicted tensile stress.

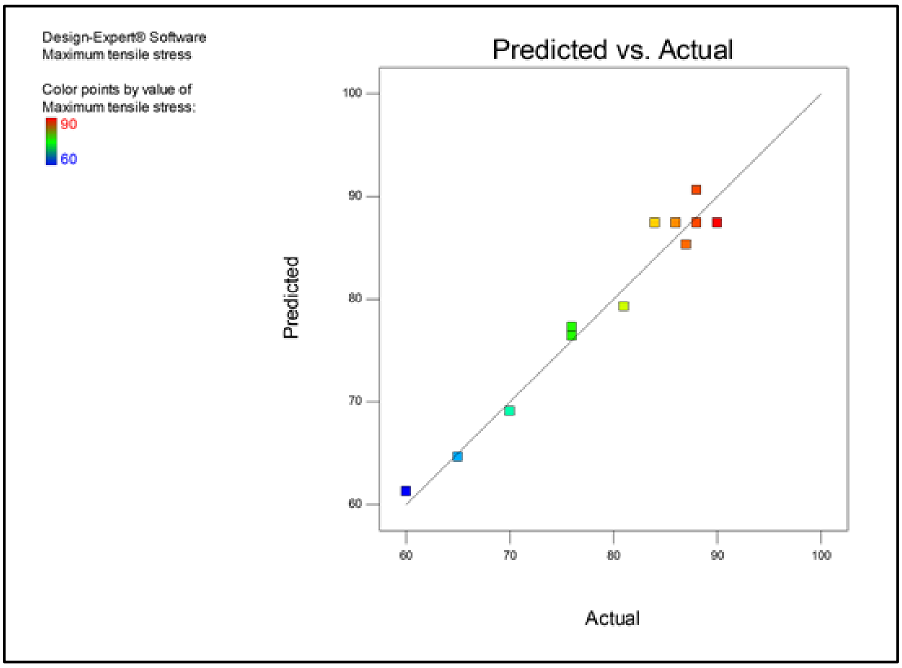

Figure 14. Predicted versus actual maximum tensile stress.

According to this figure, it can be noticed that at six Perlon layers, increasing the titanium nanoparticles individually up to 0.75% causes a slight reduction in the maximum tensile stress, while at 0.25% titanium nanoparticles, increasing the no. of Perlon layers individually up to 10 leads to decreases in the maximum tensile stress, whereas increasing both titanium nanoparticles to a higher level (0.75%) and the no. of Perlon layers being at a higher level (10 layers of Perlon) increases the maximum tensile stress to more than about 90 MPa. However, the titanium nanoparticles' percentage has a higher impact than the no. of Perlon layers on the maximum tensile stress, while the lower levels (0.25%

titanium nanoparticles and six for the no. of Perlon layers) reduce the value of maximum tensile stress.

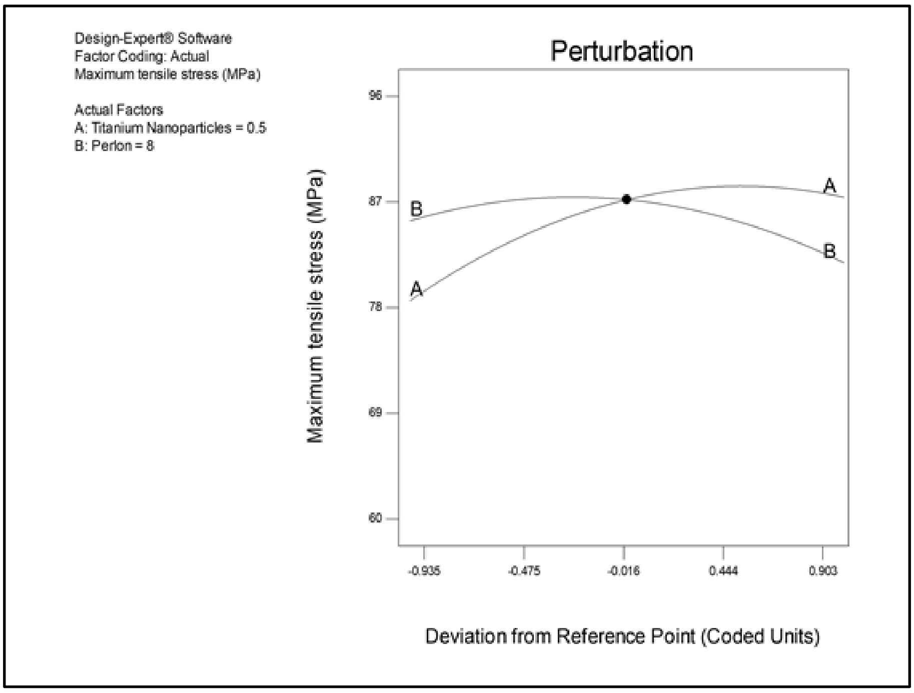

Figure 15. Perturbation of the input factors on the maximum tensile stress.

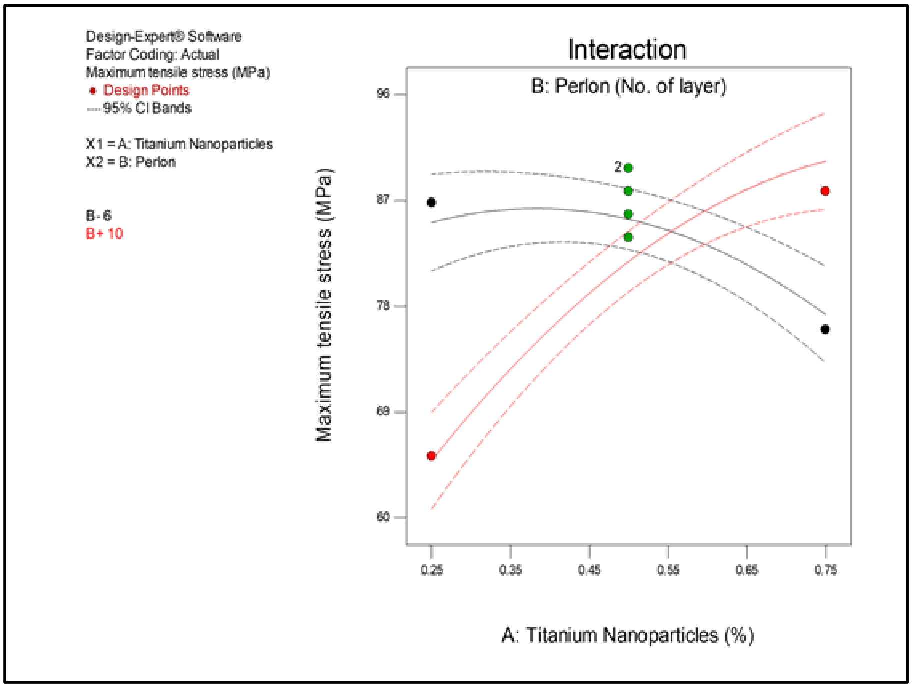

Figure 16. Interaction between the titanium nanoparticles and the no. of Perlon layers.

4.3. Results of the Maximum Bending Stress Model

In the three-point flexural test, the Testometric device was used. Each lamination material (run) with different Ti nanoparticle percentages and no. of Perlon layers was tested, and the calculated average value of the three specimens was used. It can be noted that the magnitudes of bending stress are influenced highly by the Ti nanoparticle percentage and the number of Perlon layers.

The average responses for peak bending strength were employed to determine the response surface models for each response using the least-squares approach. To predict maximum bending strength, a quadratic model reduced to coded terms was examined by reverse elimination of non-significant coefficients. At the 95% confidence level, the model is significant. The no-fit test indicates that the model is good. This results in these terms having the greatest effect on maximum bending strength, as their *p*-values are less than (0.05).

The final equation of bending strength at the peak in terms of the actual factors is:

$$\begin{gathered}\text{Bending Strength at Peak} = +178.66592 - 331.49233 \times \text{Titanium Nanoparticles} - 10.96350 \times \text{Perlon}+ \\ 42.64900 \times \text{Titanium Nanoparticles} \times \text{Perlon} - 19.31900 \times \text{Titanium Nanoparticles}^2 - 0.3377 \times \text{Perlon}^2\end{gathered} \tag{5}$$

Figure 17 shows the predicted bending strength against the actual data for comparative purposes, and Figure 18 illustrates the bending strength perturbation, which demonstrates the impact of Ti and the no. of Perlon on bending in the range of levels used; the number of Perlon layers has a more significant impact on bending than Ti. Figure 19 shows that the interrelation (combined influence) of the two input factors occurs after the center (at around 0.375 Ti% and a flexural strength of around 70 MPa).

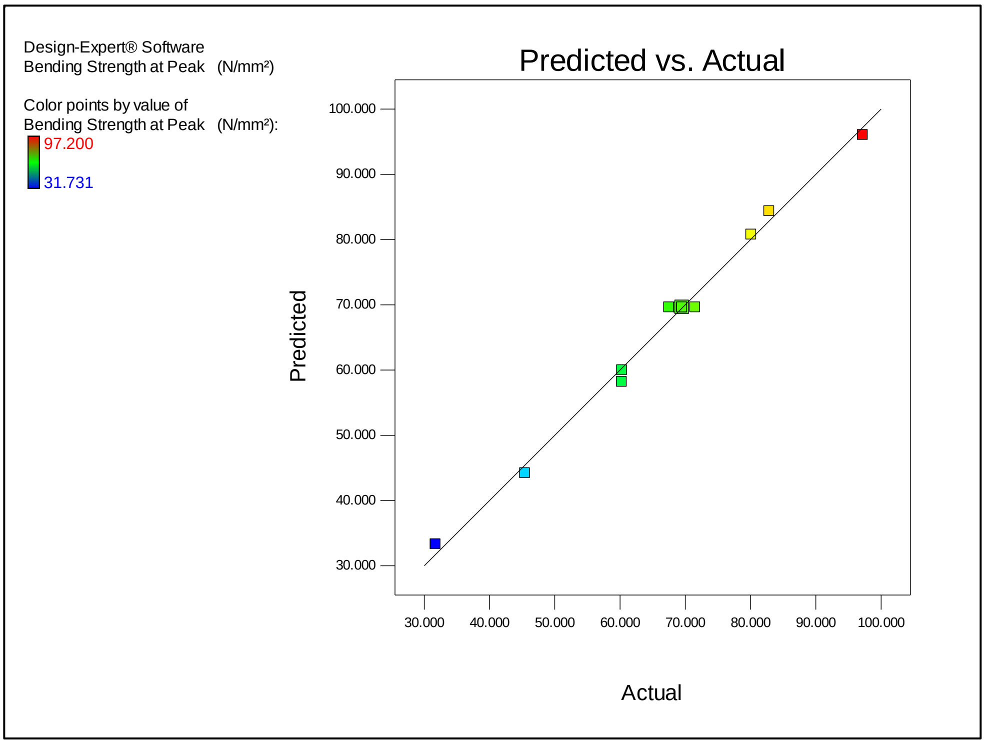

Figure 17. Predicted versus actual bending strength at the peak.

Figure 20 presents the contour plot of the titanium nanoparticle/Perlon layer interaction. The increase in titanium nanoparticles and Perlon layers increased the peak value of the bending stress, as well as the yield strength and the ultimate stress values (more than 90 MPa), which individually leads to an increase in bending. This result is likely attributed to the effect of the Ti nanoparticle % and the no. of Perlon layers, which strengthen the matrix (polyethylene) due to the formation of the higher cohesive interface between the additives (titanium nanoparticles and the no. of Perlon layers) and the matrix.

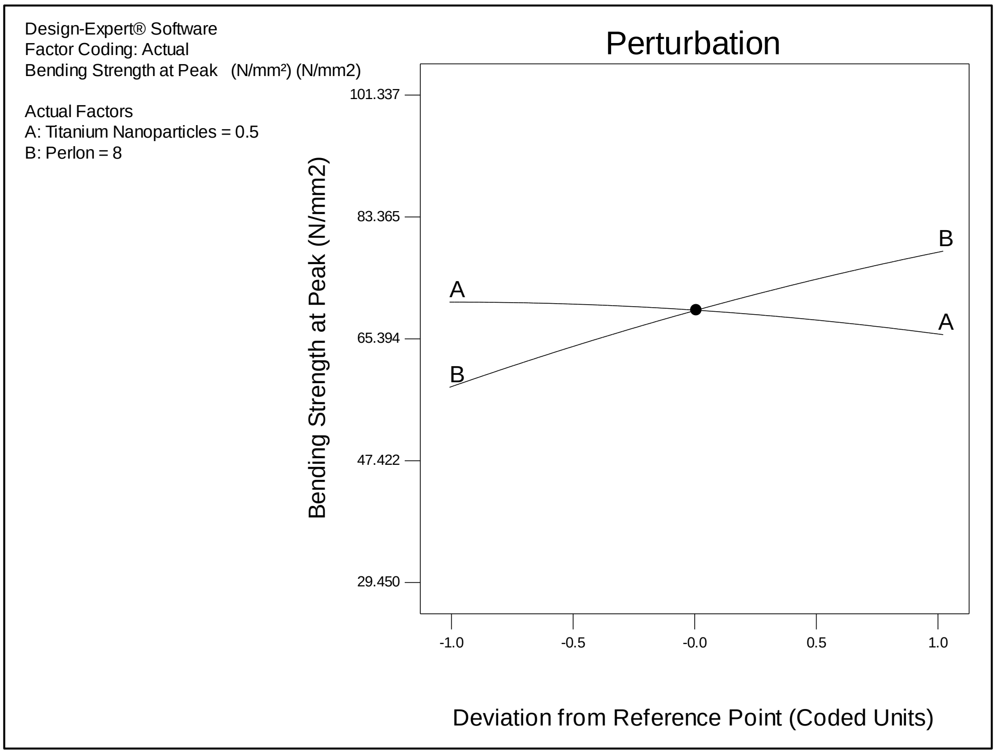

Figure 18. The bending strength at the peak perturbation of the input factors.

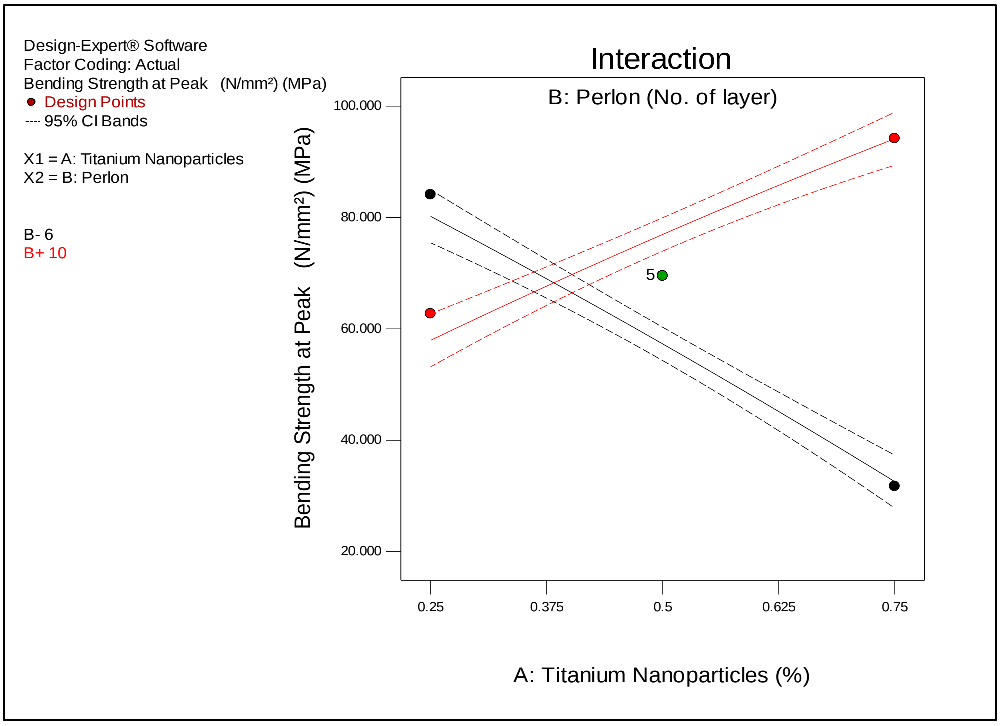

Figure 19. Interaction of the titanium nanoparticles and the no. of Perlon layers.

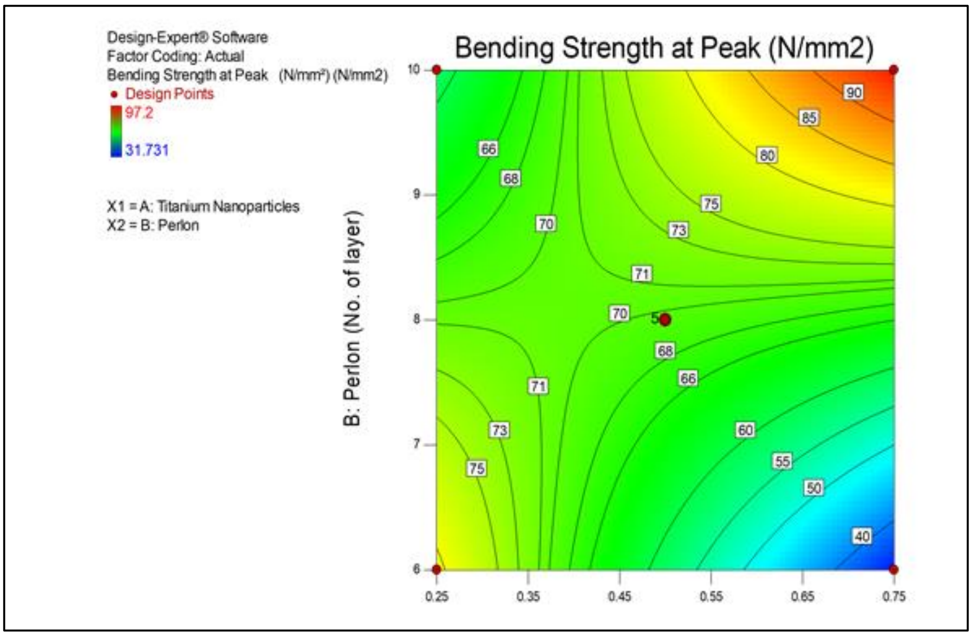

Figure 20. The 2D surface plot of bending strength at the peak in terms of the titanium nanoparticles and the no. of Perlon layers.

Figure 21 illustrates the 3D plot (surface plot) of bending strength according to Ti% and the Perlon layer number, which confirms the observations made in the 2D graph. It can be observed that increasing both Ti% and bending caused an increase in the value at their higher bending (at 10 as the no. of Perlon layers and 0.75); this is scrubbed to the same reason motioned above. On the other hand, when there is non-dispersion and insufficient adhesion between titanium nanoparticles and matrix materials, this results in a reduction in flexural properties, or a high percentage weight of titanium nanoparticles increases the viscosity of the resin and prevents the elimination of bubbles and impurities during treatment. Also, a rise in the number of Perlon layers leads to an increasing maximum bending stress value. Bending stress improves due to increasing reinforcement fiber material, which enhances the properties of composite materials and the fermion of higher cohesion of the interface between the additives (Ti nanoparticles and Perlon layers) and the matrix. These figures show that the effect of Perlon layers was the lowest when the Perlon layers were at the minimum value and the value of bending stress reached nearly (31.4 MPa) without this effect. In contrast, in titanium nanoparticles, the magnitude of maximum bending at the minimum weight percent of Ti% was high without affecting the Perlon layers.

4.4. Determination of the Optimum Input Factors, Bending at the Peak, and Maximum Tensile Stress

The design of the experiment uses the response surface methodology, which uses a central composite design for 2^2 factors, with five central points and $\alpha = \pm 2$. Thirty runs were performed according to the experimental design matrix (five center points). Each parameter was used at different code levels of -2, -1, 0, 1, and 2 whereby each level used conformed to an actual value equivalent to the coded value. The DOE software was used in the numerical optimization to determine the optimum combinations of parameters, following the specified requirements. The focus was on predicted quadratic models for the responses (bending at the tip and maximum tensile stress), with these responses modeled as functions of two input factors, namely titanium nanoparticles and the number of Perlon layers. To refine these models, a new objective function, called 'desirability', was introduced. The aim was to maximize this desirability function through numerical optimization, ranging from 0 to 1, representing the goal of obtaining the highest possible response while respecting all of the properties of the variable at the same time. Constraints for the numerical optimization of tip bending and maximum tensile stress were applied to each variable. The input factors were selected based on their usefulness, while the responses were chosen to maximize the mechanical properties, as shown in Table 4. As a result, a feasible solution satisfying these constraints was identified, resulting in maximum values for the mechanical properties (94.151 MPa peak bending strength and 90.632 MPa maximum tensile stress), as shown in Table 5. This optimum result was achieved with a maximum desirability value of 1.0, corresponding to the optimum values for titanium nanoparticles (0.75%) and the number of Perlon layers (10).

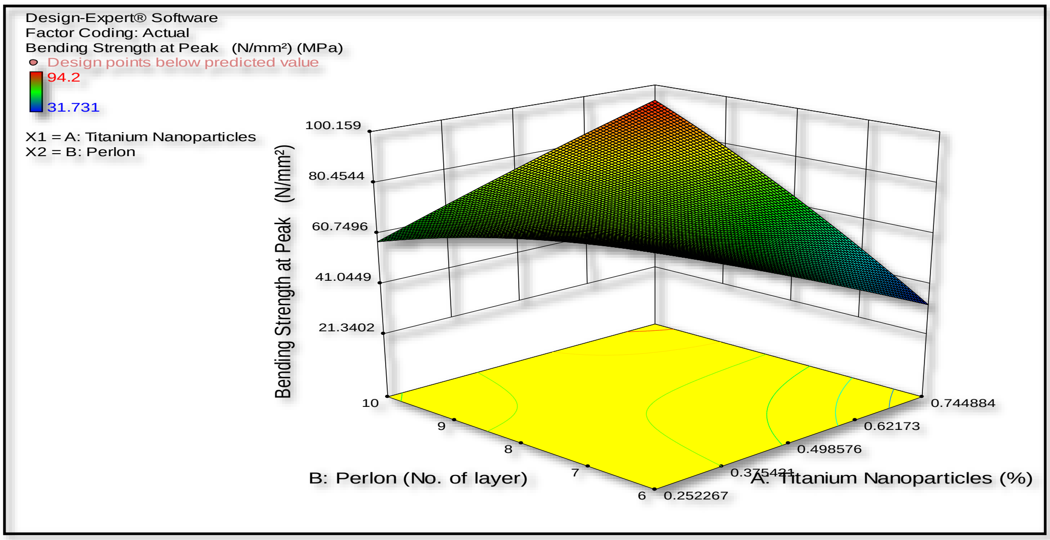

Figure 21. The 3D surface plot of bending at the peak in terms of the titanium nanoparticles and the no. of Perlon layers.

Table 4. Constraints for the numerical optimization of each variable.

Types of Variables	Goal	Lower Limit	Upper Limit	Lower Weight	Upper Weight	Importance
A: Titanium nanoparticles	It is in range	0.25	0.75	1	1	3
B: Perlon	It is in range	6	10	1	1	3
Bending strength at the Peak (N/mm^2)	Maximized	13.731	94.200	1	1	3
Maximum tensile stress (MPa)	Maximized	90	60	1	1	3

Table 5. Optimum conditions used to achieve the maximum bending at the peak and the maximum tensile stress.

Titanium Nanoparticles Percentage	No. of Perlon Layer	Bending at Break (N/mm^2)	Maximum Tensile Stress (MPa)	Desirability	Titanium Nanoparticles Percentage	No. of Perlon Layer
1	0.750	10	94.151	90.632	1.0 selected	1

4.5. Validation of the Optimum Bending at the Peak and the Maximum Tensile Stress

Confirmation tests were performed at the optimal levels of titanium and Perlon nanoparticles to confirm the maximum bending strength and the maximum tensile stress indicated in Table 5. The confirmation test results are presented in Table 6 for comparison with the experimental and predicted results. Using the results listed in this table, an error of (0.05%) and (2.90%), respectively, was found between the predicted and experimental results for maximum bending strength and maximum tensile stress.

Table 6. Comparison of experimental and predicted results for bending at maximum and maximum tensile stress.

Titanium Nanoparticles Percentage	No. of Perlon Layer	Exper. Bending at Break (N/mm^2)	Predicted Bending at Break (N/mm^2)	Exper. Maximum Tensile Stress (MPa)	Predicted Maximum Tensile (MPa)	Error (%)
0.75	10	94.200	94.151	---	---	0.05
0.75	10	---	---	88	90.632	2.90

4.6. Results of the Fatigue Test

Following the choice of optimum laminating materials based on the maximum yield strength, the ultimate tensile stress, and the maximum bending stress, the impact of the weight per unit area on the selected optimum materials, reflecting both cost and weight, was assessed through the use of two optimum design tools (titanium nanoparticles and the number of Perlon layers). The results of the fatigue tests for the optimum materials (0.75% titanium nanoparticles and 10 layers of Perlon) were also considered in the analysis. These results were compared with the previous study presented in [45]; a case of lamination materials (10 layers of Perlon) was used in this comparison.

Figures 22 and 23 illustrate the S-N plots of three different types of composite materials. Table 7 provides a fatigue life equation for the materials in each lamination. According to the figures and table, the fatigue life increased significantly in the lamination (0.75% Ti nanoparticles and 10 layers of Perlon) in comparison with the other two laminations. As a result, the optimal material proposed showed high fatigue properties with longer service life without the necessity of replacement or maintenance. In addition, the endurance stress of the optimal lamination was raised compared with the 10 layers of Perlon.

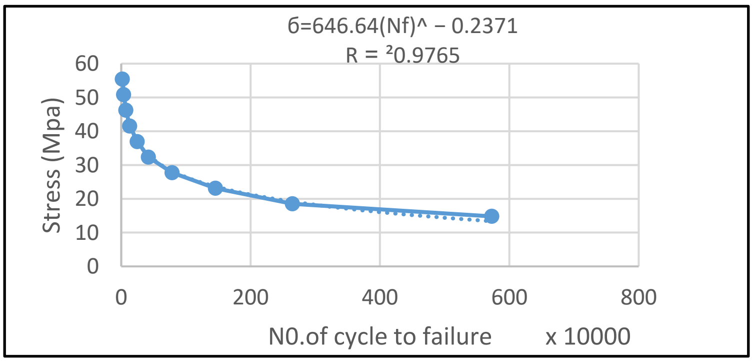

Figure 22. S-N curve for the optimal material (10 Perlon layers, 1 fiber glass, and 0.75% Ti nanoparticles).

Table 7. Fatigue life equation for the composite materials in each lamination.

Composite Material	Equation for Fatigue Life	Endurance Limits at 106 Cycles (Mpa)	R^2
10 layers of Perlon	6 = 33.64(Nf) − 0.059	15	
10 Perlon layers, 1 fiber glass, and 0.75% Ti nanoparticles	6 = 646.64(Nf) − 0.237	20	0.9765

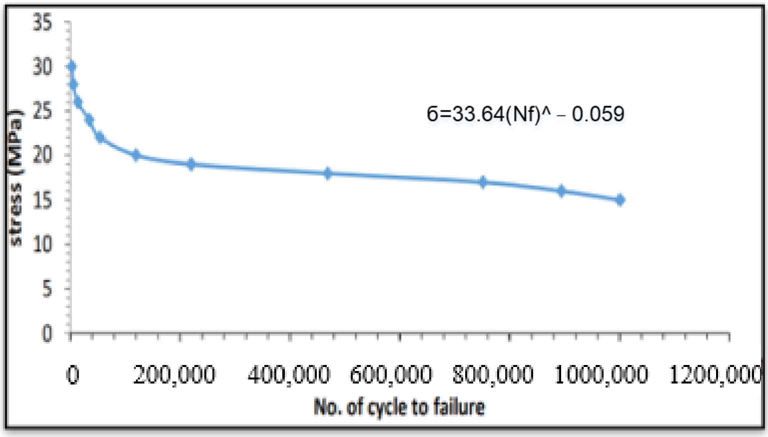

Figure 23. S-N curve for 10 layers of Perlon.

5. Conclusions

In conclusion, this study demonstrates the substantial enhancement of mechanical properties in lower limb orthoses and prostheses through the strategic integration of nanomaterials. The application of response surface methodology (RSM) yields highly accurate predictions, with a maximum error margin of only 0.05% when compared to actual experimental testing. The pivotal finding indicates that the inclusion of the suggested Ti nanoparticles significantly optimizes and bolsters mechanical attributes, particularly in conjunction with Perlon. When employing 0.75% Ti nanoparticles and 10 Perlon layers, a remarkable 40.5% increase in the fatigue endurance limit is achieved, surpassing materials commonly used at prosthetic and orthotic centers. Moreover, the study reveals that augmenting both the titanium nanoparticles percentage and the number of Perlon layers results in a notable elevation of bending strength at the peak. While the two factors exhibit an inversely proportional relationship, the influence of Perlon layers proves to be more pronounced. Their combined effect is most pronounced at approximately 0.0375% titanium nanoparticles, yielding a bending strength of about 70 MPa. Furthermore, an analogous trend is observed in the case of maximum tensile stress. An increase in titanium nanoparticle percentage and Perlon layers corresponds to an amplified maximum tensile stress. Here again, titanium nanoparticles exert a more substantial impact. The optimal combined effect is achieved at nearly 0.55% titanium nanoparticles, yielding a maximum tensile stress of about 85 MPa. Through numerical optimization, it was determined that the maximum projected values for mechanical properties stand at 95 MPa for bending strength at the peak and 90.632 MPa for maximum tensile stress. These values are attainable at the optimum proportions of 0.75% titanium nanoparticles and 10 layers of Perlon, achieving a maximum desirability value. This underscores the immense potential of this approach in advancing the field of orthotic and prosthetic manufacturing.

In summary, the use of the suggested composite material with a specific percentage of Ti nanoparticles and a specific number of Perlon layers represents a promising advance in AFO design, offering improved mechanical properties and cost efficiency.

Author Contributions: Conceptualization, N.J.K., B.L. and J.S.C.; methodology, N.J.K.; software, N.J.K. and S.B.A.; validation, N.J.K., S.B.A. and A.S.; formal analysis, N.J.K.; investigation, N.J.K., S.B.A., B.L. and J.S.C.; resources, N.J.K. and J.S.C.; data curation, N.J.K. and S.B.A.; writing—original draft preparation, N.J.K. and S.B.A.; writing—review and editing, N.J.K., S.B.A., B.L., J.S.C. and A.S.; visualization, N.J.K., S.B.A. and A.S.; supervision, B.L. and J.S.C.; project administration, B.L. All authors have read and agreed to the published version of the manuscript.

Funding: This research received no external funding.

Data Availability Statement: The raw data supporting the conclusions of this article will be made available by the authors on request.

Conflicts of Interest: The authors declare no conflicts of interest.

References

1. Cuccurullo, S.J. *Physical Medicine and Rehabilitation Board Review*; Springer Publishing Company: New York, NY, USA, 2019.
2. Natália, M.; Martins, F. Design of Ankle Foot Orthoses Using Subject Specific Biomechanical Data and Optimization Tools. Master's Thesis, Instituto Superior Técnico, Lisbon, Portugal, 2014.
3. Ben Amor, S.; Abdellaoui, S.; Tahan, A.; Louhichi, B.; Tavares, J.M.R.S. Choosing the Best Direction of Printing for Additive Manufacturing Process in Medical Applications Using a New Geometric Complexity Model Based on Part CAD Data. *Lect. Notes Comput. Vis. Biomech.* **2019**, *34*, 679–692. [CrossRef]
4. Ben Amor, S.; Zongo, F.; Eltaief, A.; Maatki, A.; Louhichi, B.; Tahan, A. A new method to select optimal part building orientation for additive manufacturing processes based on geometric complexity and heat shrinkage. *Prog. Addit. Manuf.* **2023**, *8*, 211–222. [CrossRef]
5. Rahman, M.; Zainuddin, S.; Hosur, M.; Malone, J.; Salam, M.; Kumar, A.; Jeelani, S. Improvements in mechanical and thermo-mechanical properties of e-glass/epoxy composites using amino functionalized MWCNTs. *Compos. Struct.* **2012**, *94*, 2397–2406. [CrossRef]
6. Mukherjee, T. Recent progress in process, structure, properties, and performance in additive manufacturing. *Sci. Technol. Weld. Join.* **2023**, *28*, 1–5. [CrossRef]
7. Chiad, J.S. Study the Impact Behavior of the Prosthetic Lower Limb Lamination Materials Due to Low Velocity Impactor. *J. Eng.* **2023**, *20*, 82–98. [CrossRef]
8. Mahjoob, M.; Alameer, A.K.A.; Al-Shammari, M.A. Material Characterization and Fatigue Analysis of Lower Limb Prosthesis Materials. *Assoc. Arab. Univ. J. Eng. Sci.* **2018**, *25*, 137–154.
9. Abbas, S.M.; Takhakh, A.M.; Al-Shammari, M.A.; Al-Waily, M. Manufacturing and analysis of ankle disarticulation prosthetic socket (SYMES). *Int. J. Mech. Eng. Technol.* **2018**, *9*, 560–569.
10. Qi, H.; Teo, K.; Lau, K.; Boyce, M.; Milne, W.; Robertson, J.; Gleason, K. Determination of mechanical properties of carbon nanotubes and vertically aligned carbon nanotube forests using nanoindentation. *J. Mech. Phys. Solids* **2003**, *51*, 2213–2237. [CrossRef]
11. Jber, N.R.; Rashad, A.A.; Shihab, M.S. Effects of carbon nanotubes on the physical properties of a nematic liquid crystal N-(4′-methoxybenzylidene)-4-butylaniline. *J. Mol. Struct.* **2013**, *1043*, 28–36. [CrossRef]
12. Abbas, S.M.; Resan, K.K.; Muhammad, A.K.; Al-Waily, M. Mechanical and fatigue behaviors of prosthetic for partial foot amputation with various composite materials types effect. *Int. J. Mech. Eng. Technol.* **2018**, *9*, 383–394.
13. Yaseen, N.D.; Chiad, J.S.; Ghani, F.M. The Study and Analysis of Stress Distribution Subjected on the Replacement Knee Joint Components Using Photo-Elasticity and Numerical Methods. *Int. J. Mech. Prod. Eng. Res. Dev.* **2018**, *8*, 449–464. [CrossRef]
14. Takhakh, A.M.; Abbas, S.M. Manufacturing and analysis of carbon fiber knee ankle foot orthosis. *Int. J. Eng. Technol.* **2018**, *7*, 2236. [CrossRef]
15. Yousif, L.E.; Resan, K.K.; Fenjan, R.M. Temperature effect on mechanical characteristics of a new design prosthetic foot. *Int. J. Mech. Eng. Technol.* **2018**, *9*, 1431–1447.
16. Oleiwi, J.K.; Hadi, A.N. Experimental and Numerical Investigation of Lower Limb Prosthetic Foot made from Composite Polymer Blends. *Int. J. Mech. Prod. Eng. Res. Dev.* **2018**, *8*, 1319–1330. [CrossRef]
17. Kadhim, F.M.; Takhakh, A.M.; Abdullah, A.M. Mechanical properties of polymer with different reinforcement material composite that used for fabricates prosthetic socket. *J. Mech. Eng. Res. Dev.* **2019**, *42*, 118–123. [CrossRef]
18. Abbas, E.N.; Jweeg, M.J.; Al-Waily, M. Analytical and numerical investigations for dynamic response of composite plates under various dynamic loading with the influence of carbon multi-wall tube nano materials. *Int. J. Mech. Mechatron. Eng.* **2018**, *18*, 1–10.
19. Abdulridha, M.M.; Fahad, N.D.; Al-Waily, M.; Resan, K.K. Rubber creep behavior investigation with multi wall tube carbon nano particle material effect. *Int. J. Mech. Eng. Technol.* **2018**, *9*, 729–746.
20. Taher, A.A.; Takhakh, A.M.; Thaha, S.M. Experimental study and prediction the mechanical properties of nano-joining composite polymers. *J. Eng. Appl. Sci.* **2018**, *13*, 7665–7669.
21. Oleiwi, J.K.; Afif, R.; Anaee, M. Tensile Properties of UHMWPE Nanocomposites. *J. Eng. Appl. Sci.* **2018**, 10649–10656.
22. Salih, S.I.; Oleiwi, J.K.; Ali, H.M. Investigation the properties of silicone rubber blend reinforced by natural nanoparticles and UHMWpe fiber. *Int. J. Mech. Eng. Technol.* **2019**, *10*, 164–178.
23. Salih, S.I.; Oleiwi, J.K.; Ali, H.M. Modification of silicone rubber by added PMMA and natural nanoparticle used for maxillofacial prosthesis applications. *ARPN J. Eng. Appl. Sci.* **2019**, *14*, 781–791.
24. Mohammed, A.A.; Al-Hassani, E.S.; Oleiwi, J.K. The Nanomechanical Characterization and Tensile Test of Polymer Nanocomposites for Bioimplants. In *Technologies and Materials for Renewable Energy, Environment and Sustainability: Tmrees19*; AIP Publishing: New York City, NY, USA, 2019; p. 020065.
25. Al-Waily, M.; Al-Shammari, M.A.; Jweeg, M.J. An Analytical Investigation of Thermal Buckling Behavior of Composite Plates Reinforced by Carbon Nano Particles. *Eng. J.* **2020**, *24*, 11–21. [CrossRef]
26. Rogati, G.; Caravaggi, P.; Leardini, A.; Erani, P.; Fognani, R.; Saccon, G.; Boriani, L.; Baleani, M. A novel apparatus to assess the mechanical properties of Ankle-Foot Orthoses: Stiffness analysis of the Codivilla spring. *J. Biomech.* **2022**, *142*, 111239. [CrossRef] [PubMed]

27. Shahar, F.S.; Sultan, M.T.H.; Safri, S.N.A.; Jawaid, M.; Abu Talib, A.R.; Basri, A.A.; Shah, A.U.M. Physical, thermal and tensile behaviour of 3D printed kenaf/PLA to suggest its usability for ankle–foot orthosis—A preliminary study. *Rapid Prototyp. J.* **2022**, *28*, 1573–1588. [CrossRef]
28. Patel, P.; Gohil, P. Custom orthotics development process based on additive manufacturing. *Mater. Today Proc.* **2022**, *59*, A52–A63. [CrossRef]
29. Gupta, S.; Mittal, D.; Narayan, J.; Jhunjhunwala, S.; Dwivedy, S.K. Design and Manufacturing Process of 3D Printed Ankle-Foot Orthoses for Podiatry. In *3D Printing in Podiatric Medicine*; Elsevier: Amsterdam, The Netherlands, 2023; pp. 151–173.
30. Caravaggi, P.; Zomparelli, A.; Rogati, G.; Baleani, M.; Fognani, R.; Cevolini, F.; Fanciullo, C.; Cinquepalmi, A.; Lullini, G.; Berti, L.; et al. Development of a Novel Passive-Dynamic Custom AFO for Drop-Foot Patients: Design Principles, Manufacturing Technique, Mechanical Properties Characterization and Functional Evaluation. *Appl. Sci.* **2022**, *12*, 4721. [CrossRef]
31. Khandagale, B.D.; Pise, U.V. Numerical and experimental investigation of hinged Ankle-Foot-Orthoses (AFO) using composite laminate material for Cerebral Palsy patient. *Mater. Today Proc.* **2022**, *62*, 2070–2080. [CrossRef]
32. Willis, L.; Kortobi, S.; Williams, G.; Jonaidi, M.; Nasseri, S. Design, Finite Element Analysis and Fabrication of Composite Orthoses for Bunions; A Comprehensive Study. *Int. J. Prod. Sound Qual.* **2023**, *1*, 59–77. [CrossRef]
33. Luo, Z.; Wang, Z.; Xu, B.; Sarakiotis, I.; Du Laing, G.; Yan, C. Measurement and characterization of engineered titanium dioxide nanoparticles in the environment. *J. Zhejiang Univ. Sci. A* **2014**, *15*, 593–605. [CrossRef]
34. Wolfram, J.; Zhu, M.; Yang, Y.; Shen, J.; Gentile, E.; Paolino, D.; Fresta, M.; Nie, G.; Chen, C.; Shen, H.; et al. Safety of Nanoparticles in Medicine. *Curr. Drug Targets* **2015**, *16*, 1671–1681. [CrossRef]
35. Al-Waily, M.; Deli, A.A.; Al-Mawash, A.D.; Ali, Z.A.A.A. Effect of natural sisal fiber reinforcement on the composite plate buckling behavior. *Int. J. Mech. Mechatron. Eng.* **2017**, *17*, 30–37.
36. Kadhim, A.A.; Al-Waily, M.; Ali, Z.A.; Jweeg, M.J.; Resan, K.K. Improvement fatigue life and strength of isotropic hyper composite materials by reinforcement with different powder materials. *Int. J. Mech. Mechatron. Eng.* **2018**, *18*, 77–86.
37. Sadiq, S.E.; Jweeg, M.J.; Bakhy, S.H. The Effects of Honeycomb Parameters on Transient Response of an Aircraft Sandwich Panel Structure. *IOP Conf. Ser. Mater. Sci. Eng.* **2020**, *928*, 022126. [CrossRef]
38. Abbas, H.J.; Jweeg, M.J.; Al-Waily, M.; Ali Diwan, A. Experimental Testing and Theoretical Prediction of Fiber Optical Cable for Fault Detection and Identification. *J. Eng. Appl. Sci.* **2019**, *14*, 430–438. [CrossRef]
39. Abbod, E.A.; Al-Waily, M.; Al-Hadrayi, Z.M.; Resan, K.K.; Abbas, S.M. Numerical and Experimental Analysis to Predict Life of Removable Partial Denture. *IOP Conf. Ser. Mater. Sci. Eng.* **2020**, *870*, 012149. [CrossRef]
40. Sadiq, S.E.; Bakhy, S.H.; Jweeg, M.J. Effects of spot welding parameters on the shear characteristics of aluminum honeycomb core sandwich panels in aircraft structure. *Test Eng. Manag.* **2020**, *83*, 7244–7255.
41. Mansoor, H.I.; Al-Shammari, M.A.; Al-Hamood, A. Experimental analysis of cracked turbine rotor shaft using vibration measurements. *J. Mech. Eng. Res. Dev.* **2020**, *43*, 294–304.
42. *ASTM D638-14*; Standard Practice for Preparation of Metallographic Specimens. American Society for Testing and Materials International: West Conshohocken, PA, USA, 2016; Volume 82, pp. 1–15.
43. *ASTM D790-03*; American Society for Testing and Materials Information, Handing Series "Standard Test Method for Flexural Properties". American Society for Testing and Materials International: West Conshohocken, PA, USA, 2000.
44. *ASTM D790*; Standard Test Methods for Flexural Properties of Unreinforced and Reinforced Plastics and Electrical Insulating Materials. American Society for Testing and Materials International: West Conshohocken, PA, USA, 2019.
45. Abdul-Kareem, H.S.; Abdulla, F.A.; Abdulrazzaq, M.A. Effect of Shot Peening and Solidification on Fatigue Properties of Epoxy Base Composite Material. *IOP Conf. Ser. Mater. Sci. Eng.* **2019**, *518*, 032017. [CrossRef]